

CHALMERS



Method for Total Air Flow Prediction in Compartment A Numerical Study of the Climate System at Volvo Car Corporation *Master's thesis in Applied Mechanics*

MARTIN SVENSSON

Department of Applied Mechanics
Division of Fluid Mechanics
CHALMERS UNIVERSITY OF TECHNOLOGY
Göteborg, Sweden 2013
Master's thesis 2013:78

MASTER'S THESIS IN APPLIED MECHANICS

Method for Total Air Flow Prediction in Compartment

A Numerical Study of the Climate System at Volvo Car Corporation

MARTIN SVENSSON

Department of Applied Mechanics
Division of Fluid Mechanics
CHALMERS UNIVERSITY OF TECHNOLOGY
Göteborg, Sweden 2013

Method for Total Air Flow Prediction in Compartment
A Numerical Study of the Climate System at Volvo Car Corporation
MARTIN SVENSSON

© MARTIN SVENSSON, 2013

Master's thesis 2013:78
ISSN 1652-8557
Department of Applied Mechanics
Division of Fluid Mechanics
Chalmers University of Technology
SE-412 96 Göteborg
Sweden
Telephone: +46 (0)31-772 1000

Chalmers Reproservice
Göteborg, Sweden 2013

Method for Total Air Flow Prediction in Compartment
A Numerical Study of the Climate System at Volvo Car Corporation
Master's thesis in Applied Mechanics
MARTIN SVENSSON
Department of Applied Mechanics
Division of Fluid Mechanics
Chalmers University of Technology

ABSTRACT

To predict and control the total amount of air passing through the ventilation system is of great importance when designing and developing climate systems for the automotive industry. There are clear benefits both concerning the climate comfort in the compartment and cost efficiency in the development process, if the flow in an early stage can be estimated and analysed virtually. This project is a part of the development work of a computational method to be used for flow rate prediction of the climate system in the automotive industry at the Volvo Car Corporation (VCC).

The new method consists of guidelines for setting up a numerical model of the climate system and directives on how to carry out the flow rate computations. The climate system refers to the complete internal system for transporting air through the vehicle compartment. In this thesis however, a model of the VCC climate test rig was used instead of a complete car model in order to simplify the verification. Since the amount of air transported through the system is assumed to be closely connected with the performance of the fan, emphasis was directed towards the modeling of the centrifugal fan. For this purpose a steady state approach, using multiple reference frames (MRF) to deal with the fan rotation, was used. Also, a minor investigation of the solution's mesh dependency and the dependency towards choice of turbulence model ($k - \varepsilon$ standard, $k - \varepsilon$ realizable and $k - \omega$ SST) was performed.

In order to evaluate the method the mass flow through the VCC test rig was measured and compared with the computational model. The CFD simulations of the system modeled with ≈ 54 million cells, $k - \varepsilon$ realizable as turbulence model and with the fan at maximum operating speed showed promising results and exceeded the measurements only by 2% but due to leakage in the test set up this value can not be regarded as completely reliable. Instead of a slight overprediction, the CFD results would probably underpredict the flow without the leakage since the measured values would most likely be significantly larger.

Even though the results appear to correspond to the measured values some further validations are suggested. There are some uncertainties connected to the measurements both considering leakage and the blower speed estimation that need to be clarified. Some effort may also be reserved to ensure an unambiguously grid independent solution and try the model for different operational fan speed and system resistance.

Keywords: centrifugal fan, CFD, climate comfort, HVAC, MRF

ACKNOWLEDGEMENTS

I wish to acknowledge the support of persons who have helped me complete this project. First of all, I would like to recognise the support of my supervisor, Johan Levin. Thank you for great support and for giving me the opportunity to develop this master thesis into my own project. Thanks to my supervisor and examiner, Lars Davidson, who helped to lead the work forward when doubtfulness was upon me. I also would like to direct a special thanks to Shayan Rahat who provided excellent comments on the work and helped me with both editorial and theoretical aspects. Finally, I want to express my warmest gratitude to all of you working at the CFD-group for your hospitality and friendly environment. You made me feel as a part of the group from day one and you made it easier to handle those days when I was hopelessly stuck in the numerics.

NOMENCLATURE

Abbreviations

CAD	Computer Aided Design
CFD	Computational Fluid Dynamics
DNS	Direct Numerical Solution
MRF	Multiple Reference Fram
VCC	Volvo Car Corporation
HVAC	Heating, Ventilation, and Air Conditioning
LES	Large Eddy Simulation
SST	Shear Stress Transport

Roman Characters

f_i	Body force in the x_i direction
g	Gravitational acceleration
k	Turbulent kinetik energy
P_s	Static pressure
P_t	Total pressure
S_i	Source term in the x_i momentum equation
u	Streamwise velocity
u_τ	Frictional velocity
u^+	Non-dimensional streamwise velocity
v_i	Velocity (in direction i)
\hat{v}_i	Time-averaged velocity
v'_i	Fluctuating velocity
x_i	Coordinate in x_i th direction
y	Wall distance (normal to wall)
y^+	Non-dimensional wall distance
z	Height over ground

Greek Characters

β	$= -\frac{1}{\rho} \left(\frac{\partial \rho}{\partial T} \right)_p$
δ_{ij}	Kronecker delta
ε	Dissipation
μ	Dynamic viscosity
μ_t	Turbulent dynamic viscosity
ν	Kinematic viscosity
ν_t	Turbulent kinematic viscosity
ρ	Density
τ_{ij}	Stress tensor
ω	$= \frac{\varepsilon}{kC_\mu}$

Empirical Constants

$1/\alpha$	$= 41000000$
C_2	$= 1350$
C_μ	$= 0.09$
$C_{\varepsilon 1}$	$= 1.44$
$C_{\varepsilon 2}$	$= 1.92$
σ_k	$= 1.00$
σ_ε	$= 1.30$
κ	$= 0.41$
B	$= 5.1$

CONTENTS

Abstract	i
Acknowledgements	iii
Nomenclature	v
Contents	vii
1 Introduction	1
1.1 Problem Statement	1
1.2 Purpose	1
1.3 Limitations	1
2 Theory	3
2.1 The Climate System	3
2.1.1 Fan Performance	4
2.2 The Physics and the Computational Model	5
2.2.1 Basic CFD	5
2.2.2 Modelling the Fan	8
3 Method	11
3.1 Measuring the Mass Flow in the VCC Test Rig	11
3.2 Setting up the Computational Model	11
4 Results and Discussion	15
4.1 Air Flow through the Climate System	15
4.2 Fan Model Robustness	17
4.2.1 Differences due to Geometry and Mesh Changes	17
4.2.2 Differences due to Turbulence Models	18
5 Conclusions	22
5.1 Recommendations	22
References	23
Appendix A - Mesh Density	I
Appendix B - Measurement	III

1 Introduction

The requirements of the climate system of today's cars are indeed tough. Although the purpose, to provide a comfortable environment for the passengers, is the same the means of doing so have changed over time. There are of course many possibilities connected with the development of new techniques such as active control and automatically tuned regulators, but there are also some difficulties arising with the new technology. Especially the pursuit of lowering energy consumption makes some features problematic that were previously solved naturally. The engines of modern cars are developed to minimize heat losses, so there is now less waste heat available for heating the compartment and defrosting the windshield. It is therefore essential to develop an efficient and intelligent climate system to reach the goals of lowering fuel consumption and at the same time provide a comfortable climate for the customer.

In order to design a climate system that could handle these challenges it is important to fully understand and control the flow passing through the car and optimize the components to minimize losses and maximize efficiency. There are several ways to get there, testing and measuring is one way to gain knowledge about the system. Another important instrument is to use computational methods and in this way predict the flow characteristics. A great advantage of using the virtual alternative is the possibility to capture the main features of the flow in an early stage of the development and make proactive improvements and in that way reduce the time and expense for testing and measuring.

1.1 Problem Statement

This project aims to predict the total amount of air that passes through the compartment using CFD utilities and will be a part of the method development for complete vehicle climate analysis at Volvo Car Corporation.

1.2 Purpose

Today's requirements on the climate system at Volvo Car Corporation are mainly expressed as pressure drops over ducts and components and air distribution in the nozzles. The existing computational methods correspond to these requirements but the ambition of the VCC climate department is to prescribe a required air flow into the compartment, and with the current methods this cannot be evaluated computationally. Therefore, a new method will be developed where the fan is included so that the actual volume flow rate can be predicted. Previous studies of the fan performance and CFD models trying to mimic the fan characteristics show promising results and demonstrate the potential gain in modeling the climate system numerically, [10], [5].

Even though a major part of this thesis is focused on modelling the centrifugal fan and to study parameters that presumably affect the airflow, the overall purpose is to contribute to the method development including the complete climate system. Therefore, it is also desirable to avoid making the model too computationally expensive.

1.3 Limitations

This project includes only the components directly influencing the flow through the climate system. No consideration will be taken to thermodynamic properties such as humidity effects and condensation. In other words, the air will be treated as dry adiabatic. In order to reduce the complexity of the model and simplify the verification process the complete car will not be modelled but only the climate system as it is mounted in VCC's climate system test rig.

2 Theory

This chapter aims to introduce the reader to the background needed to fully acquire the results and conclusions. In Section 2.1 a brief introduction of the climate system and fan performance will be held and in Section 2.2 the physics behind the computations and some numerical models will be explained. If the reader is already familiar with any of these areas that section can be omitted. However, it is recommended to look through Section 2.1 about the climate system to get an idea about the orientation and notation of the different components as these will be referred to later in the report.

2.1 The Climate System

The climate system refers to the complete internal system for transporting air through the car. In this project the modeled climate system has a slightly different configuration namely that of the VCC climate test rig. Schematic pictures of the complete system can be seen in Figure 2.1a and the test rig can be seen in Figure 2.1b. A more detailed description of the test is presented in Section 3.1.

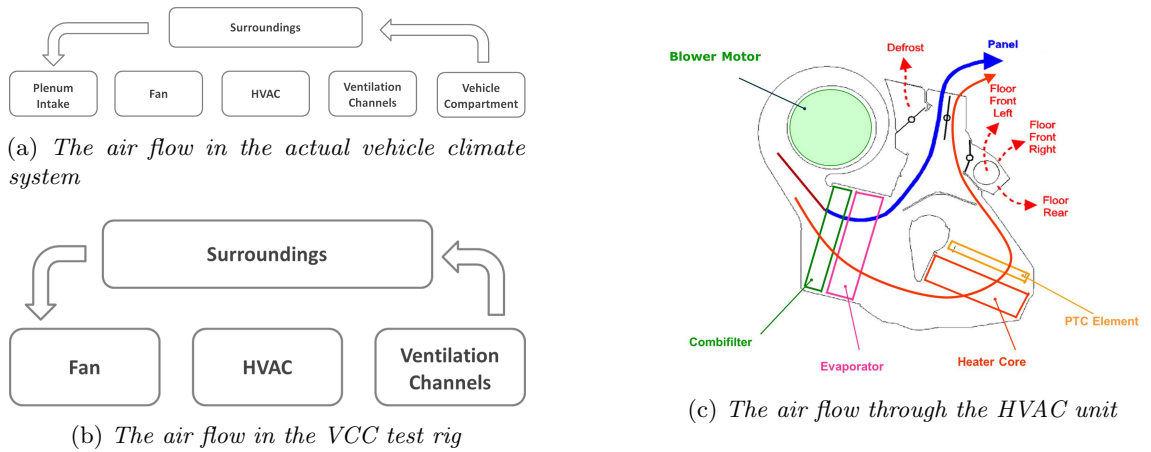


Figure 2.1: Schematic illustrations of the climate system and its components

For the real car system the air flows from the surroundings through the plenum intakes, via an air filter and into the fan. The air continues through the HVAC (Heating, Ventilation, and Air Conditioning) unit where it is distributed depending on which ventilation mode that is requested. The HVAC unit includes all the different elements that makes changes in the compartment climate possible, locally or globally. Among other things the HVAC unit contains the evaporator that absorbs thermal energy from the air and different heater elements that add thermal energy to the air. After the HVAC the air goes through different ventilation ducts that distribute the air into the compartment. A schematic figure of the HVAC unit can be seen in Figure 2.1c.

The components of the climate system can be seen in Figure 2.2a and Figure 2.2b and in Figure 2.3 the complete climate system is shown.



(a) The fan cover with the air filter in blue and centrifugal blower in red (b) The HVAC-unit with the evaporator in purple and outlet to panel ventilation in orange

Figure 2.2: Components of the climate system

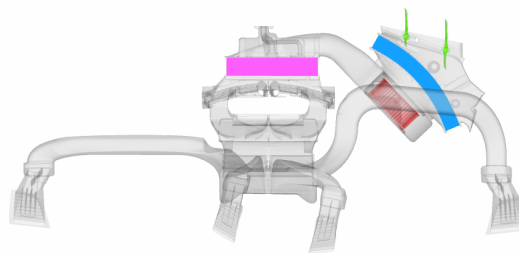


Figure 2.3: The complete front ventilation configuration

When dealing with internal flows it is convenient to study the total pressure variation through the system. The total pressure is defined as

$$P_t = P_s + \frac{1}{2}\rho v^2 + \rho g z \quad (2.1)$$

and is the sum of the properties defining the state in the Bernoulli's principle. The total pressure should therefore remain constant when following a streamline for incompressible, adiabatic flow where no external work or any pressure losses are affecting the system. Such pressure losses are always present in practical applications and can be either frictional losses or losses caused by spatial changes in the geometry. The total pressure is therefore a good tool for evaluating the resistance of a system and is frequently used as a key parameter when designing climate systems for automotive purpose. More details about pressure drops in channels with different geometries can be found in [11] and information about fluid mechanics in general can be found in [17].

2.1.1 Fan Performance

The characteristics of the fan may vary depending on type and environment. In [15] and [8] a brief overview is given and in [10] a more detailed study of the aerodynamic aspects can be found. Here, a brief introduction to the characteristics of a forward curved fan will be presented, since this is the type of fan used in the project. A sketch of the forward curved fan is shown in Figure 2.4a and a typical forward curved fan performance curve is shown in Figure 2.4c.

The curve of Figure 2.4c is obtained by separating the fan inlet from the outlet by placing the suction side in a chamber and then restrict the incoming air to the chamber, see Figure 2.4b. When varying the restriction there will be a pressure difference between the suction side, P_1 , and the pressure side, P_2 , of the fan. If the inflow to the chamber is completely restricted there will be a vacuum on the suction side leading to zero airflow

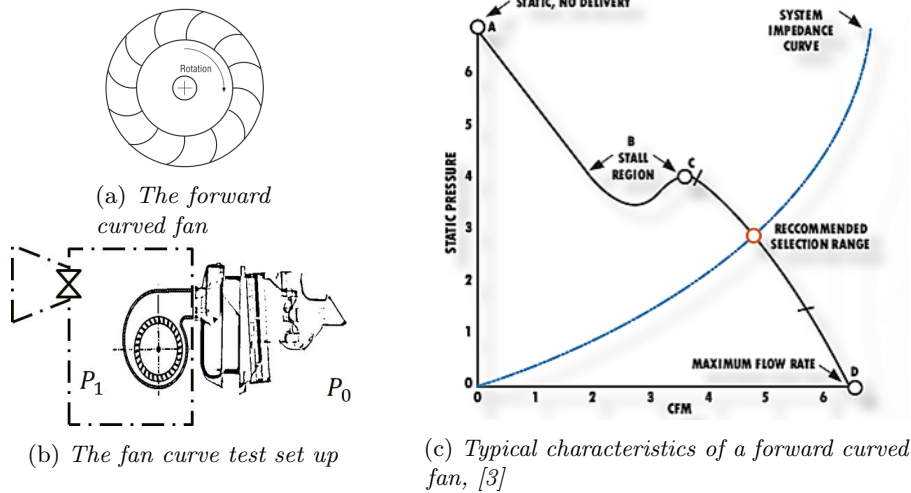


Figure 2.4: Fan performance curve

and a large pressure difference between the chamber and the surrounding air, point A. When the restriction is decreased the flow rate is increasing and pressure drop is decreasing following the curve. When the restriction is zero there will be no pressure difference between incoming air and surrounding air, point D. The fan has an unsteady region in point B where a single pressure matches three different flow rates. This behavior is important to take into account when modelling the fan since it most likely is connected to large amounts of turbulence.

2.2 The Physics and the Computational Model

In order to predict the flow characteristics the principles of the fluid dynamics have to be expressed mathematically. The fundamental principles governing the flow are

- conservation of mass (continuity)
- the rate of change in momentum is equal to the sum of all forces acting on the fluid element (Newton's second law)
- conservation of energy (first law of thermodynamics)

These principles combined with some thermodynamic relation fluid properties (equation of state) are the cornerstones of the fluid dynamics and can be used to describe the flow field. In this project the most important variables are the velocity and the pressure. The flow field is also affected by changes to properties of the fluid itself but for simplicity these are assumed not to influence the flow for this particular problem significantly and the properties can therefore be treated as constants.

The mathematical expression of the governing principals can for simplified cases be solved analytically but for practically all industrial cases the equations have to be solved numerically using methods combined under the term Computational Fluid Dynamics or CFD.

2.2.1 Basic CFD

A detailed discussion of CFD is beyond the scope of this report. However, it can be suitable to get some basic knowledge on the subject to get better insight about the project's outcome. For further information on the subject there are a number of introductory literature, for instance References [16] and [4].

When solving the flow field there are several ways to express the equations governing the flow. The most convenient way to write them is in primitive form, solving for the velocity and pressure. This makes the boundary conditions straightforward but does make the equations a bit problematic to solve. In Equations 2.14,

2.15 and 2.4 the governing equations are written on primitive form for an incompressible flow using cartesian coordinates. For information about tensor notation see Reference [7].

$$\frac{\partial v_i}{\partial x_i} = 0 \quad (2.2)$$

$$\frac{\partial v_i}{\partial t} + v_j \frac{\partial v_i}{\partial x_j} = f_i - \frac{1}{\rho} \frac{\partial p}{\partial x_i} + \nu \frac{\partial^2 v_i}{\partial x_j^2} \quad (2.3)$$

$$\rho c_p \frac{\partial T}{\partial t} + v_i \rho c_p \frac{\partial T}{\partial x_i} = \Phi + \frac{\partial}{\partial x_i} \left(k \frac{\partial T}{\partial x_i} \right) \quad (2.4)$$

These equations are based on the principals of fluid dynamics. Equations 2.14 and Equation 2.15 are often referred to as the Navier-Stokes equations and describe mass conservation and rate of change in momentum respectively. Equation 2.4 is the energy equation and is connected with the momentum equation via the Φ term that contains an expression for the dissipation. Since the temperature has no significant effect on the velocity field in this particular case Equation 2.4 will not be treated further. For more information on dissipation and the use of the energy equation see [6] chapter 2.2 and [16] chapter 2.1.

Ignoring Equation 2.4, there are four equations and four unknowns (v , u , w and p) meaning that this system can be solved assuming appropriate boundary conditions are provided. However, these equations are often rewritten for a turbulent case using the velocity decomposition $v = \bar{v} + v'$, where \bar{v} is the mean velocity and v' is the velocity fluctuations. The same decomposition can be applied to the pressure so that $p = \bar{p} + p'$. Using the decomposed velocity and pressure and time averaging Equations 2.14 and 2.15 gives

$$\frac{\partial \bar{v}_i}{\partial x_i} = 0 \quad (2.5)$$

$$\bar{v}_j \frac{\partial \bar{v}_i}{\partial x_j} = f_i - \frac{1}{\rho} \frac{\partial \bar{p}}{\partial x_i} + \frac{\partial}{\partial x_j} \left(\nu \frac{\partial \bar{v}_i}{\partial x_j} - \overline{v'_i v'_j} \right) \quad (2.6)$$

This set of equations are called the Reynolds-Averaged Navier-Stokes (RANS) equations. It should be mentioned that this is not the only way to solve the turbulent flow field. The most straightforward way is to actually solve the entire flow directly from 2.15, including the turbulent fluctuations, but due to the scales of the smallest turbulent structures (eddies) this would require a very fine grid and extremely small time steps and is therefore not yet suitable for industrial purpose. Another alternative is to resolve some of the eddies and model the ones the grid can not resolve. This strategy requires solving of the unsteady flow equations and is therefore demanding in terms of computational power. Even though the computational resources are sufficient to run transient simulations it is often desirable with a steady solution and therefor only the steady state RANS turbulence models will be discussed further. More information about different turbulence methods can be found in [16] chapter 3.6.

Note that Equation 2.15 and 2.6 are almost exactly the same but the term $-\frac{\partial}{\partial x_j} \overline{v'_i v'_j}$ is added due to the stresses caused by turbulent interactions on the mean velocity field. Now there is one more unknown term added and it is no longer possible to close the equation system. To solve the equations something needs to be done to deal with this new term. There are a some different approaches to solve this problem and once again it is not possible to describe these entirely in this report. Here, only the most common ones or the ones most appropriate for this particular case will be presented. These are the $k - \varepsilon$ model, the $k - \varepsilon$ realizable model and the $k - \omega$ SST model and are all based on the idea of turbulent viscosity. The $-\frac{\partial}{\partial x_j} \overline{v'_i v'_j}$ term represents stresses on the fluid element from the interacting turbulent fluctuations, $\tau_{ij} = -\rho \overline{v'_i v'_j}$. For the viscous stress Newton's law of viscosity states that the stress tensor, τ_{ij} , is proportional to the rate of deformation of the fluid element, [16].

$$\tau_{ij} = \mu \left(\frac{\partial v_i}{\partial x_j} + \frac{\partial v_j}{\partial x_i} \right) \quad (2.7)$$

It would be convenient to use a similar expression for the turbulent stresses $-\rho \overline{v'_i v'_j}$ since this would solve the problem with the extra unknown in Equation 2.6. Boussinesq's assumption provides such a relationship so that

$$-\rho \overline{v'_i v'_j} = \mu_t \left(\frac{\partial \bar{v}_i}{\partial x_j} + \frac{\partial \bar{v}_j}{\partial x_i} \right) - \frac{2}{3} \rho k \delta_{ij} \quad (2.8)$$

The need for the extra term $-\frac{2}{3}\rho k\delta_{ij}$ is discussed in [16]. Equation 2.8 introduces a new parameter, the turbulent viscosity μ_t and if this quantity were known then it would be possible to close the flow equations. In addition to μ_t there is also the kinematic turbulent viscosity, $\nu_t = \frac{\mu_t}{\rho}$. The next sections will give a brief presentation of the most commonly used models for the turbulent viscosity.

$k - \varepsilon$ model standard model

The standard $k - \varepsilon$ model is based on dimensional analysis to find an expression for the turbulent viscosity so that

$$\mu_t = \rho C_\mu \frac{k^2}{\varepsilon} \quad (2.9)$$

where $k = \frac{1}{2}(\bar{v}_1'^2 + \bar{v}_2'^2 + \bar{v}_3'^2)$ is the turbulent kinetic energy and ε is the dissipation. In the $k - \varepsilon$ model two new transport equations are used for these quantities. A transport equation is in general formed in the following fashion using Φ as an unknown quantity

$$\begin{array}{ccccc} \text{Rate of} & & \text{Transport} & & \text{Transport} & & \text{Rate of} & & \text{Rate of} \\ \text{Change of} & + & \text{of } \Phi \text{ by} & = & \text{of } \Phi \text{ by} & + & \text{production} & - & \text{destruction} \\ \Phi & & \text{convection} & & \text{diffusion} & & \text{of } \Phi & & \text{of } \Phi \end{array}$$

and the transport equations for the standard $k - \varepsilon$ model are the k -equation, [6],

$$\frac{\partial k}{\partial t} + \bar{v}_j \frac{\partial k}{\partial x_j} = \nu_t \left(\frac{\partial \bar{v}_i}{\partial x_j} + \frac{\partial \bar{v}_j}{\partial x_i} \right) \frac{\partial \bar{v}_i}{\partial x_j} - \varepsilon + \frac{\partial}{\partial x_j} \left[\left(\nu + \frac{\nu_t}{\sigma_k} \right) \frac{\partial k}{\partial x_j} \right] \quad (2.10)$$

and the ε -equation, [6]

$$\frac{\partial \varepsilon}{\partial t} + \bar{v}_j \frac{\partial \varepsilon}{\partial x_j} = \frac{\varepsilon}{k} C_{\varepsilon 1} \nu_t \left(\frac{\partial \bar{v}_i}{\partial x_j} + \frac{\partial \bar{v}_j}{\partial x_i} \right) \frac{\partial \bar{v}_i}{\partial x_j} - C_{\varepsilon 2} \frac{\varepsilon^2}{k} + \frac{\partial}{\partial x_j} \left[\left(\nu + \frac{\nu_t}{\sigma_\varepsilon} \right) \frac{\partial \varepsilon}{\partial x_j} \right] \quad (2.11)$$

$C_\mu, C_{\varepsilon 1}, C_{\varepsilon 2}, \sigma_k$ and σ_ε in these equations are constants. The standard $k - \varepsilon$ is a widely used turbulence model since it is simple to implement, fast and is validated for many different types of flows. However, it shows poor performance in, for example rotational flow, adverse pressure gradient flow and boundary layer flows, [16].

$k - \varepsilon$ realizable model

The realizable $k - \varepsilon$ is based on the standard $k - \varepsilon$ model but does include some new features. The same expression for the turbulent viscosity is used but this time the C_μ is not constant and another transport equation for ε is used, [1]. The new transport equation, that will not be stated here, is derived from the transport equation of vorticity fluctuation. This model has shown superior behavior to the standard $k - \varepsilon$ model in predicting problems including rotating flow and flow with strong curvature but since the model of the turbulent viscosity includes effects of the mean rotation the realizable $k - \varepsilon$ should be used with some caution when used in combination with multiple reference frames, [1].

$k - \omega$ SST model

The $k - \omega$ SST model is a combination of the benefits from the standard $k - \omega$, see [16] chapter 3.7, near the boundary layer and the stability of the $k - \varepsilon$ in the free stream. This makes the model more accurate than the standard $k - \varepsilon$ model and more reliable than the standard $k - \omega$ model. The model is well suited for solving flows including adverse pressure gradients where the $k - \varepsilon$ shows unsatisfying results. For more details and further reading about turbulence modeling see [6], [16], [12] and [1].

Wall Functions

An other important fact to consider before moving on is the wall boundary condition. On the wall, both the normal and the tangential velocity has to be zero to fulfill the no-slip condition but what value shall the first cell adjacent to wall take? The inner boundary layer of a fully developed turbulent flow can be divided into three different zones; the viscous sublayer, the buffer region and the logarithmic region, [6]. In the viscous sublayer the influence of turbulence can be neglected and the flow is assumed to be laminar. In the logarithmic region the flow is dominated by turbulence and in the buffer layer the flow is influenced by both viscous and turbulent diffusion and the velocity is therefore hard to predict. There are therefore two alternatives for the first cell placement, either it is placed in the viscous subregion or in the logarithmic region where the velocity profile can be estimated.

The suitable distance to the wall for these regions is determined by the non-dimensional wall distance, $y^+ = \frac{u_\tau y}{\nu}$ where $u_\tau = \sqrt{\frac{\tau_w}{\rho}}$ and $\tau_w = \mu(\frac{\partial u}{\partial y})_{y=0}$. When the first node is located in the viscous sublayer, $y^+ \approx 1$, the following equation can be used to determine the velocity of the first cell.

$$u^+ = \frac{u}{u_\tau} = y^+ \quad (2.12)$$

For the logarithmic region, $30 \lesssim y^+ \lesssim 3000$, a logarithmic wall function shall be used

$$u^+ = \frac{u}{u_\tau} = \frac{1}{\kappa} \log(y^+) + B \quad (2.13)$$

where κ and B are empirical constants, [6].

2.2.2 Modelling the Fan

Generally there are three different ways to handel the total pressure increase caused by the fan. The choice of fan model is, as for many CFD problems, a trade off between accuracy and computational effort but the appropriacy of a certain method is also dependent on the application. For a highly unsteady flow there is for instance little chance to get satisfying results with a steady simulation.

Pressure Jump

The simplest way to model the fan would be to represent it as a sudden pressure jump, that may or may not vary with the flow velocity, Figure 2.5. This approach may be used to get a rough approximation of the total pressure and capacity of a system driven by a fan but it will not include any swirling motion of the fluid. For this model experimental data on the fan performance is needed to specify the fan behavior.

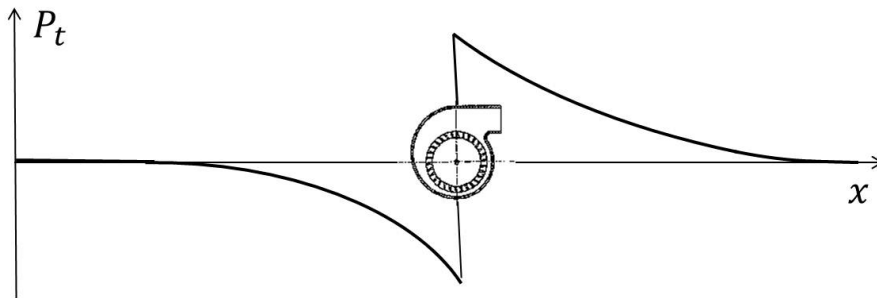


Figure 2.5: Sketch of the total pressure over the fan

MRF

The second way to model the fan is to use a rotating reference system for the rotating parts. Rotating boundary conditions are used inside the rotation domain and the centripetal acceleration and Coriolis acceleration are included in the governing equations so that the flow "feels" the forces of the rotation even though the fan does not actually move. The governing equation for the steady, incompressible MRF approach are, [1] chapter 2.2.

$$\frac{\partial v_{ri}}{\partial x_i} = 0 \quad (2.14)$$

$$\frac{\partial v_{ri} v_j}{\partial x_j} + \epsilon_{ijk} \omega_j v_k = f_i - \frac{1}{\rho} \frac{\partial p}{\partial x_i} + \nu \frac{\partial^2 v_i}{\partial x_j^2} \quad (2.15)$$

where the relative velocity, $v_{ri} = v_i - u_{ri}$, v_i is the absolute velocity and u_{ri} is the velocity due to the rotating reference frame.

This way of modelling rotating bodies are often referred to as Frozen Rotor approach or Multiple Reference Frame (MRF) and is used in many different applications for rotating problems. Since the MRF approach gives a steady state solution and the fan does in reality rotate some physical phenomena can not be evaluated using this approach but the fact that it is steady state is also appealing considering the large amount of computational time needed for transient simulations. Reports on whether MRF is a suitable strategy for modelling these types of problems show varying results. In [13] the MRF approach shows good resemblance to the experimental results and in [5] the result is promising as long as the resistance (pressure drop) in the system is not too large. On the other hand, in [9] the MRF approach shows a slight under prediction and in [10] the a MRF solution could not be converged.

Sliding Mesh

The third way is to run a transient simulation where the mesh round the rotating part actually moves with the blades. This should be the most robust strategy, [2], but it is also unambiguously the most time consuming. In the sliding mesh setup the fluid domain is divided into one rotating mesh and one stationary mesh. The meshes are then sliding along the interface with the rotational velocity of the fan. For more detail on the sliding mesh technique see [1] chapter 3.2.

3 Method

The total amount of air flowing through the compartment was analysed using CFD utilities. It is important to remember that the results from these computations do not actually describe the flow through the car itself but through the VCC climate test rig. Therefore, some words about the test, the computational model and the validity of this approach should be mentioned. Also, some settings and inputs for the computational model will be presented in this chapter.

3.1 Measuring the Mass Flow in the VCC Test Rig

The measurement in the VCC climate test rig included the major part of the climate system but was lacking the plenum inlet and the actual car compartment. Instead, the air entered directly through the air filter and evacuated through the nozzles into the surrounding room. The HVAC was set to front ventilation mode, meaning that the air did not enter any heater element and that only the first row panel ducts were opened. With this configuration no regard could be taken to the pressure inside the compartment or inlet pressure variations due to the car motion but for the purpose of evaluating the computational model the test rig was considered a suitable reproduction of the climate system. The components included in the test set up can be seen in Figure 3.1a.

The mass flow through each one of the four panel ventilation nozzles was measured using hot wire mass air flow (MAF) sensors, see [14], and summed to get the total air flow (see Appendix 2 for measurement data). Significant leakage was detected in the test leading to a discrepancy between measurements and computations since it was not possible to include this leakage in the computational model. The leakage was estimated to be greatest at the second row ventilation ducts (B-pillar) and in order to reduce the effects of the leakage the flow rate through these ducts were also measured and added to the results. The rotational speed of the fan was calculated based on the fan power input and not measured. There is a contingency in computing the rotational velocity in this way but due to limited measuring time and measuring tools it was not possible to directly measure the fan velocity. These issues make the accuracy of the test unsatisfactory but the measurements can still be used as an indication of the flow rate through the compartment.

3.2 Setting up the Computational Model

To be able to predict the airflow through the climate system the fan was considered of particular interest and therefore a separate study of some fan parameters was performed including mesh dependency and dependency to choice of turbulence model. It was of course important to model the entire system accurately. If the pressure drop over the ventilation channel for instance would be too high due to some nonphysical resistance in the system the fan would be too weak for the purpose of overcoming this resistance and the flow rate would be wrongly estimated.

The computational model is as mentioned a model of the VCC test rig and includes air filter, blower, HVAC including evaporator, panel ventilation ducts and outlet nozzles. Figure 3.1a shows the essential parts included in the computational model and Figure 3.1b shows the connection to the surrounding environment.

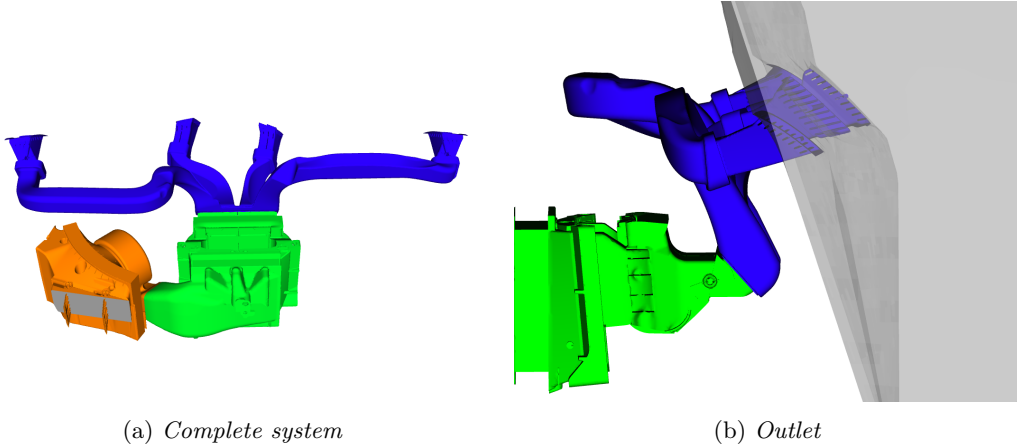


Figure 3.1: Computational domain

In Figure 3.1a the fan cover (containing air filter and the fan itself), the HVAC and the first row panel ventilation channels can be seen in orange, green and blue respectively. The gray surface on the fan cover is where the air entered the system from the inlet box. The inlet surrounding and the outlet surrounding were not connected to each other as they were in the test but they were separated in different boxes (the outlet box can be seen in Figure 3.1b). At the inlet, the total pressure was set to zero and at the outlet boundary the static pressure was set to zero making the fan the only driving force of the flow.

The fan was modeled using the MRF approach in order to keep the computational time at a reasonable level. The ambition was initially to compare the MRF with the sliding mesh technique but no such simulation could be carried out. Since the maximum ventilation mode was assumed to be the most demanding, the work was focused on simulations with high blower speeds, i.e 3300 rpm. When simulating lower fan velocities the solution was less stable possibly due to large scale transient flow.

The air filter and the evaporator were modeled with the porous media approach in Fluent, adding a source term to the flow equations representing both the viscous resistance (first term on in Equation 3.1) and the inertial resistance (second term in Equation 3.1) of the filter as

$$S_i = \left(\frac{\mu}{\alpha} v_i + C_2 \frac{1}{2} \rho |v| v_i \right) \quad (3.1)$$

Both the viscous- and the inertial resistance were assumed to be a factor 100 times larger in the tangential directions.

The CAD geometry was cleaned in the pre-processing tool ANSA version 14.0.0, from which a surface representation was exported. The volume mesh was created using HARPOON v5.0a. HARPOON is an octree mesher, that creates a hexadominant mesh starting from a coarse grid throughout the domain and gradually refining the mesh towards the surfaces. The characteristics of the octree method makes it possible to create a large mesh for a complex geometry relatively fast but the surface representation and boundary layer control can be suffering since the mesh is refined towards the surface instead of expanding from the surface. The computation was carried out using the ANSYS Fluent solver and post processed in EnSight.

A minor investigation on the sensitivity to the mesh density and turbulence model was performed. The turbulence models of choice were as mentioned the standard $k - \varepsilon$, the realizable $k - \varepsilon$ and the $k - \omega$ SST model. The realizable $k - \varepsilon$ case was modeled with three different mesh densities to investigate the mesh dependency. The fine mesh that was used contained ≈ 37 million cells and a low density mesh contained ≈ 10 million cells. A

second fine mesh, ≈ 38 million cells, was built on a rougher surface representation with coarser surface elements around the blades. The intention was to keep a y^+ near 1 primarily at the blades with all meshes so that the linear wall function could be used. (In Fluent the enhanced wall function is the near wall alternative and is said to be valid even outside the viscous sublayer ($y^+ > 5$), [2]). Out of curiosity also the logarithmic wall function was used for two of the meshes. For details on the mesh see Appendix B - Measurement. The model of the complete climate system contained ≈ 54 million cells (using the ≈ 37 million cell model for the fan).

4 Results and Discussion

The results are divided into two sections. First, in Section 4.1, a comparison between the measurements described in Section 3.1 and the CFD results will be presented. Also, CFD results from the existing method predicting the air flow distribution at VCC (where the fan is not included) will be compared with the new method (including the fan) to see if including the fan in the model will change the distribution in the ventilation nozzles. In 4.2 some differences in the fan model performance due to changes in either mesh or turbulence model are shown. The purpose of this visualization is to decide how robust the modelling of the fan is and which parameters affect the flow the most.

4.1 Air Flow through the Climate System

When comparing the CFD model with the measurement it is important to have in mind the inevitable differences between these. The CFD model is based on a CAD geometry that can never entirely coincide with the actual geometry. There is significant leakage in the real climate system that is not accounted for in the CFD model. Also, the air filter and the evaporator are, as mentioned in Section 3.2 modelled as porous regions and not as exact reproduction of the geometry. The CFD model is most definitely an estimation of the real climate system test rig and the question is how good that estimation is.

The distribution of the panel ventilation and the total flow rate at maximal blower speed is presented in Table 4.1, difference from measured value in parenthesis. In the present method at VCC the flow into the HVAC is assumed to be uniformly distributed at the inflow but in the method including the fan this is not the case as can be seen in Figure 4.1. This difference may suggest a potentially improved estimation of the air flow distribution and outflow directability using a computational method including the fan but according to Table 4.1 this improvement is not evident. Both methods overpredicts the flow through the center passenger nozzle and underpredicts the flow through the side passenger nozzle. If anything the new method suits the measurement better but due to uncertainties in the measurements this tendency is very vague.

Table 4.1: Air distribution in ventilation nozzles

	Driver Side	Driver Center	Pass. Center	Pass. Side
Measurement	22.4 %	24.6 %	28.9 %	24.1%
CFD With Fan Model	23.0 % (+0.6)	25.0 %(+0.4)	30.8 % (+1.9)	21.2 % (-2.9)
CFD Mass Flow Inlet	21.6 % (-0.8)	26.3 % (+1.7)	31.2 % (+2.3)	20.9 % (-3.2)

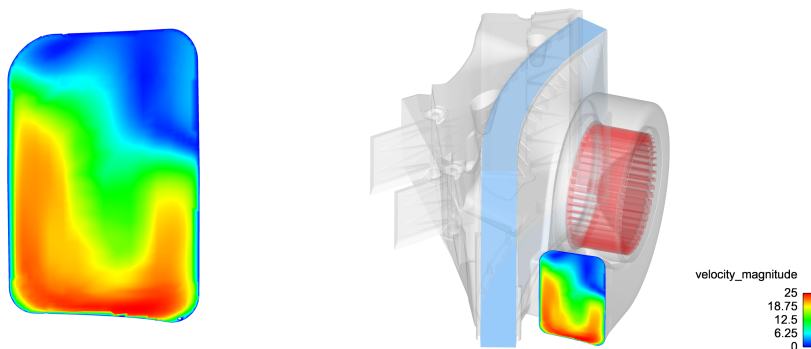


Figure 4.1: *Velocity contour at fan outlet*

The air flow through the climate system is shown in Table 4.2. If only the second row is taken into account then the CFD model differs considerably from the measurements. The reason for the large difference is that the leakage of the HVAC and ventilation channels is not included in the CFD model. As mentioned in section Section 3.1 the leakage is most severe to the second row and if that leakage is included the air flow amounts

correspond much better. It should be mentioned that there was leakage not only to the second row but this was the only leakage large enough to measure properly. The measured airflow should therefore most likely be higher than the value in Table 4.2 leading to a possible underprediction in the CFD model.

Table 4.2: Air distribution in ventilation nozzles

	1st Row	Leakage to 2nd Row	Total Air Flow
Measurement	87 l/s	17 l/s	104 l/s
CFD With Fan Model	106 l/s	-	106 l/s (+2%)

In Figure 4.2 the flow through the system is illustrated using streamlines. (The ventilation ducts are placed separately and scaled for clarity). The air filter and the evaporator are restricting the flow only to run in the normal direction which causes some problems in the simulations. To get a stable solution the simulation has to be started without the air filter and after a couple of hundred iterations the filter can be included. The air goes through the HVAC without passing the heating elements. Instead it runs through the side channels on its way to the panel ventilation ducts.

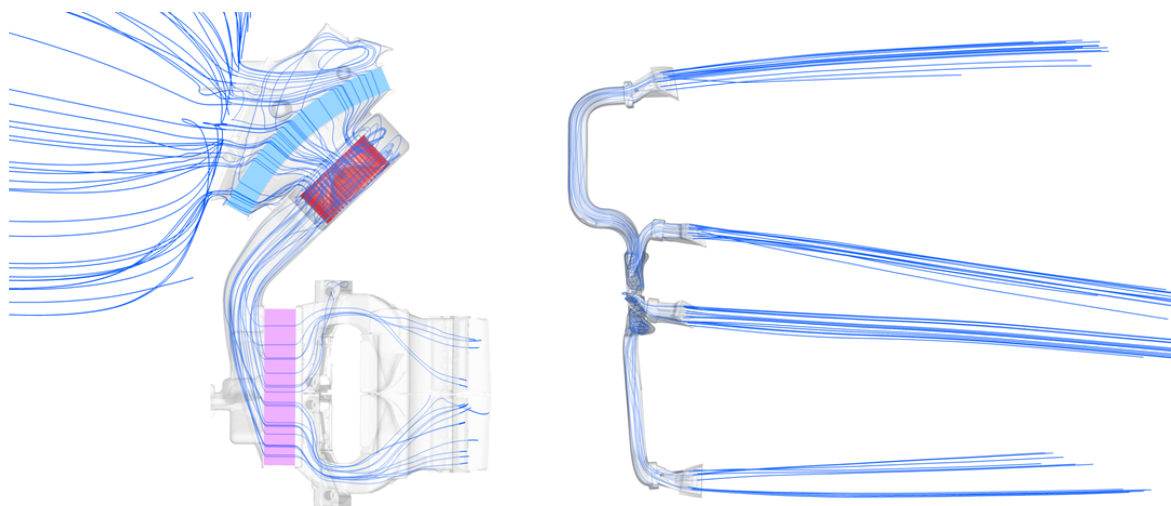


Figure 4.2: *Streamlines through the system*

The total pressure losses in the climate system cause a resistance for the fan to overcome. If this resistance is big the flow rate is decreasing and this may cause instabilities in the flow. One way to investigate if this is the case is to look at the total pressure around the blower. If the total pressure is positive in the inner region of the fan this is an indication of reversed flow and unsteadiness, [5]. Since the MRF approach is a steady simulation this behavior would signal when it might be necessary to switch from the MRF approach to the sliding mesh. Figure 4.3 shows the total pressure around the blower.

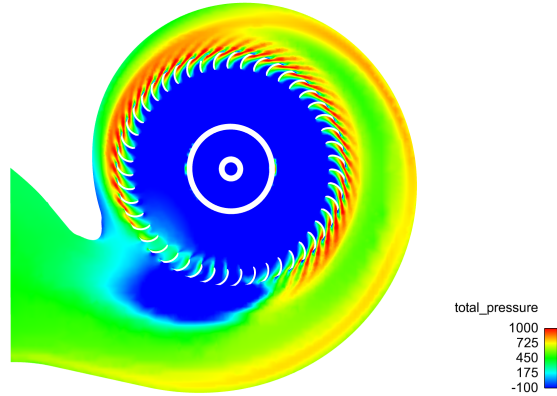


Figure 4.3: *Total pressure*

There is some recirculation caused by the cut-off edge (baffle) forcing the air into the blower wheel and the total pressure in this region is positive. Since the phenomenon is very weak this potentially unsteady behavior does most probably not cause any significant errors to the steady solution.

4.2 Fan Model Robustness

The dependency to mesh density and choice of turbulence model is evaluated only on the isolated fan since the fan is assumed to be the most important part for the air flow calculation. The fan is the only part that has not been included in any VCC climate comfort method before. It is also convenient not to include a too large model in the parameter study considering computer requirements.

4.2.1 Differences due to Geometry and Mesh Changes

Figure 4.4 shows the mass flow for three different meshes. An overview description of the meshes is given in Table 4.3. For further details on the different meshes see Appendix A - Mesh Density.

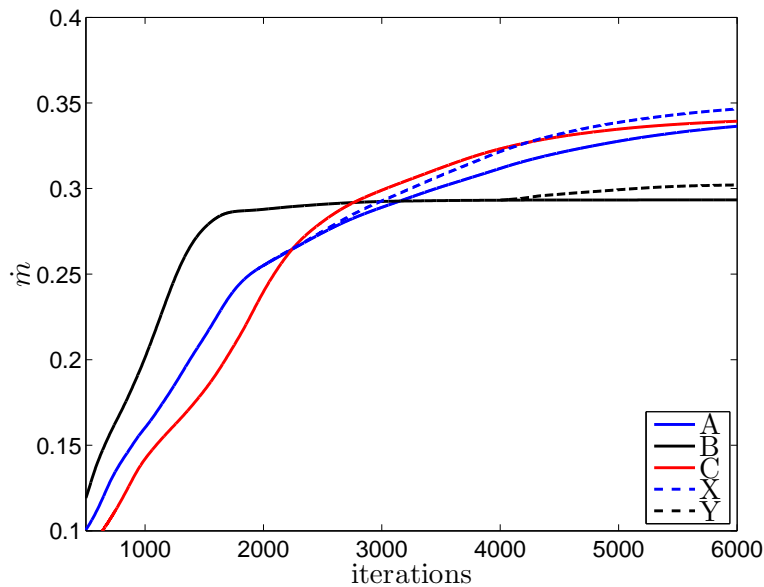


Figure 4.4: *Mass flow for different meshes*

Table 4.3: Declaration of cases with different meshes

A	A high density mesh with ≈ 37 M cells Prism layer on fan blades Enhanced wall function used for approximating the velocity in the first cell
B	A low density mesh with ≈ 10 M cells No prism layer Enhanced wall function
C	A high density mesh with ≈ 38 M cells but with coarser surface representation No prism, instead constant expansion from the blade surface was used Enhanced wall function
X	Same as A but logarithmic wall function
Y	Same as B but logarithmic wall function

The low density mesh is fully converged at approximately 2000 iterations while the high density meshes require at least 6000 iterations. There is a $\approx 16\%$ difference in the mass flow between the low density mesh and the high density meshes. The high density meshes give similar results. This is somewhat surprising since case C is meshed on a surface not capable of representing the blade curvature as well as case A (can be seen in Figure 4.5). Case C is also meshed without a prism layer closest to the wall resulting in cells outside of the preferred $y^+ \approx 1$ distance, see Figure 4.5c. Instead of a prism layer, the height of the cells closest to the wall are restricted to not exceed the width of the surface cell. In Figures 4.5a, 4.5b and 4.5c the y^+ for case A, B and C are shown and the effect of the prism layer is very clear.

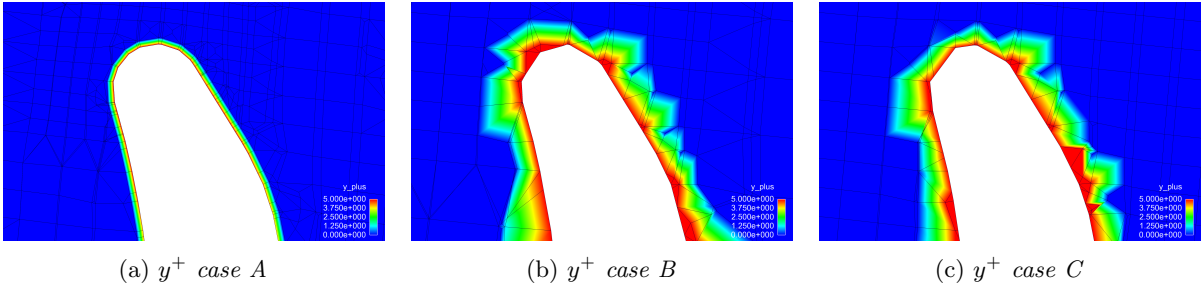


Figure 4.5: y^+ for three different meshes

4.2.2 Differences due to Turbulence Models

The mass flow of three cases with different turbulence models are shown in Figure 4.6. All cases are based on the same mesh (case A Table 4.3).

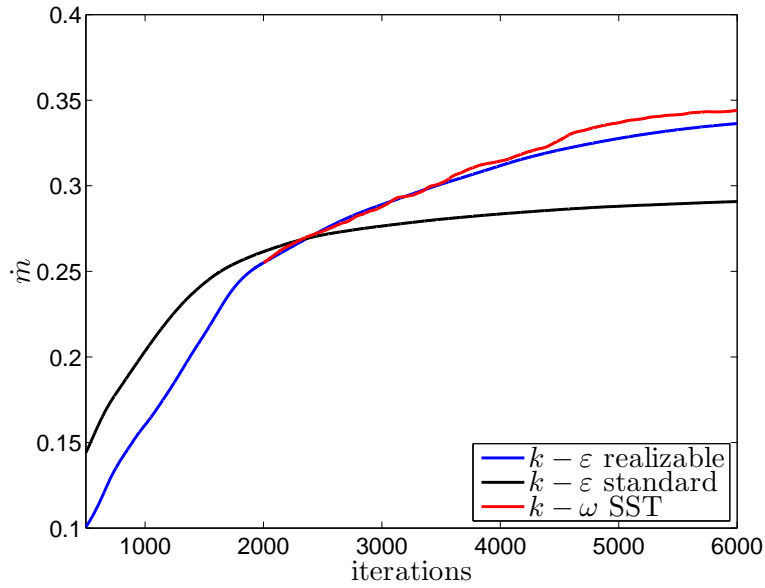


Figure 4.6: Mass flow for different turbulence models

There is a clear difference ($\approx 18\%$) between the $k - \epsilon$ standard and the other two models. As mentioned in Section 2.2.1 the standard $k - \epsilon$ should, according to literature, perform poorly in rotational flows and this is probably what causes the low volume flow. The other two models are in very close agreement but the $k - \omega$ SST is not very stable. In fact, the simulation had to be started using a realizable $k - \epsilon$ model for 2000 iterations otherwise the simulation would diverge.

A more detailed investigation of the behavior of the turbulence models is given below. The sections that are studied are shown in Figure 4.7.

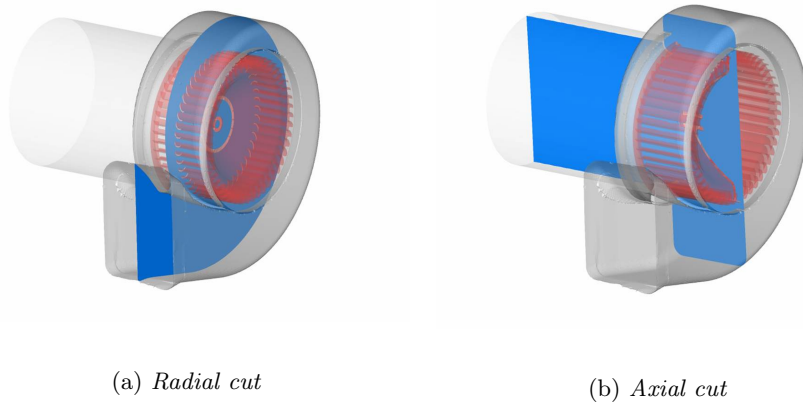


Figure 4.7: Cuts for post-processing

In Figure 4.8 the turbulent kinetic energy, $k = \frac{1}{2} \overline{v'_i v'_i}$, for the $k - \epsilon$ realizable, $k - \epsilon$ standard and $k - \omega$ SST model is shown respectively. Even though the equation for the turbulent kinetic energy is expressed in the same way for all these turbulence models the difference in the calculation of the turbulent viscosity, μ_t , leads to some differences in this quantity.

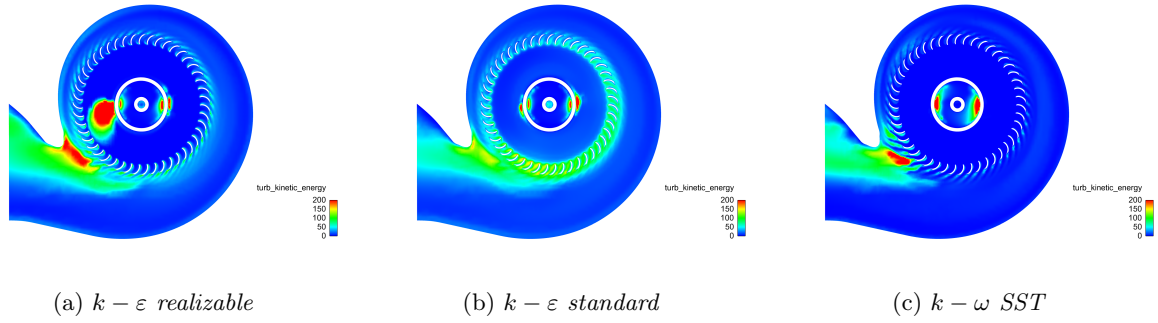
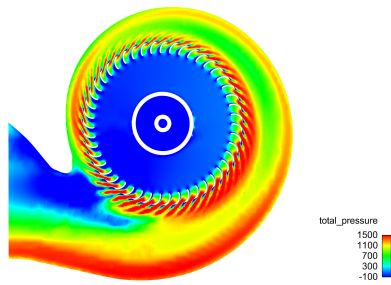


Figure 4.8: *Turbulent kinetic energy*

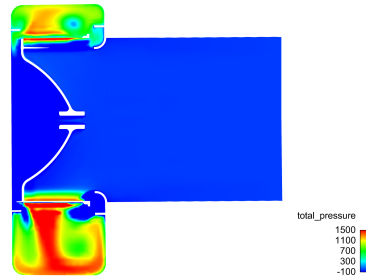
The $k - \epsilon$ realizable and $k - \omega$ models once again show similar results. A high normal stress area is present close to the cut-off edge and at the trailing edge of the blade in these two models. In the standard $k - \epsilon$ the turbulent kinetic energy is more concentrated to the blower wheel. As mentioned in Section 2.2 the standard $k - \epsilon$ has problems in adverse pressure gradient flow such as flow around the airfoils of the blower where the turbulent viscosity is overpredicted (and therefore also the turbulent shear stress). This might lead to the blower "carrying" a lot of air inside the blower, reducing the amount of air that is actually leaving the blower, resulting in a lower total flow rate for this model than for the others. In all three models, there is a region inside the blower with locally high turbulence which may be the result of some numerical issue.

Figure 4.9 shows the total pressure around the blower for the different turbulence models. If the total pressure is positive in the inner region of the fan this is an indication of reversed flow and unsteadiness. Since the MRF approach is a steady approximation this behavior would signal when it might be necessary to switch from the MRF to the sliding mesh approach. In this case the blower is operating at a very stable high air flow region (near operating point D in Section 2.1.1). Compare these figures with Figure 4.3 where the system resistance is higher and a tendency towards positive total pressure in the interior parts of the blower is visible.

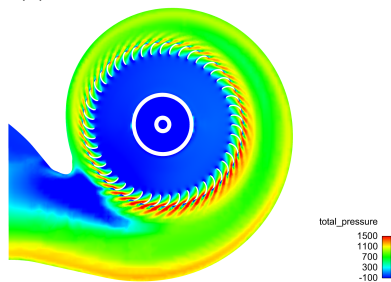
The pattern is similar in all models but total pressure in the standard $k - \epsilon$ model is more smeared out than the others and the total pressure increase due to the fan is also lower. This is another indication of lower velocities in the standard $k - \epsilon$ model.



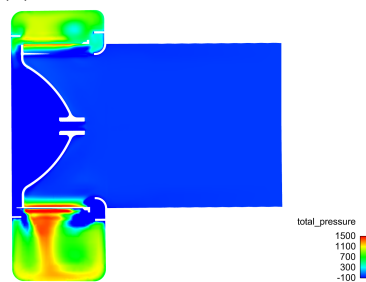
(a) *Radial cut realizable $k - \epsilon$*



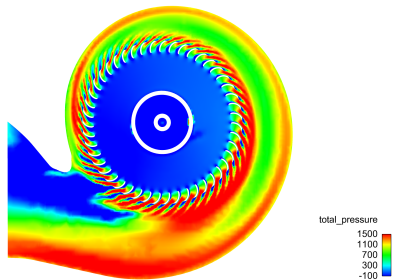
(b) *Axial cut realizable $k - \epsilon$*



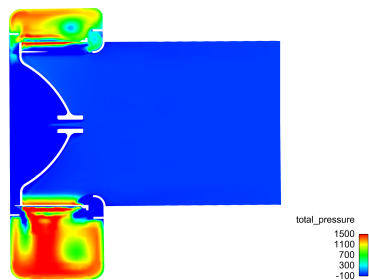
(c) *Radial cut standard $k - \epsilon$*



(d) *Axial cut standard $k - \epsilon$*



(e) *Radial cut $k - \omega$ SST*



(f) *Axial cut $k - \omega$ SST*

Figure 4.9: *Total pressure*

5 Conclusions

Considering the results of this project there seems to be no reason to not include the fan in the development and evaluation of the climate system and the MRF appears to be a suitable approach for the fan model. The results from the CFD model exceeded the measurements by only 2%. However, the MRF approach should be used with some caution when modeling systems with high resistance and low flow rate. The flow in such cases is more likely to show large scale transient behavior and the MRF approach is not longer suitable.

The new method, including the fan, might be a good approach for providing information about the total flow rate through the compartment but does not add any significant improvements for simulating the air distribution and directability. For these purposes the current method, using a uniform mass flow as inlet condition, is suitable.

The realizable $k - \varepsilon$ turbulence model shows good results compared to the standard $k - \varepsilon$ model and is more stable than the $k - \omega$ SST model and therefore a suitable choice for the method.

There is a large difference between the fine mesh and the coarse mesh that is probably caused by the difference in resolution near the blade. If the near blade region is not sufficiently refined the momentum transferred via viscosity from the blades to the fluid surrounding it will be underestimated, since this transfer is dependent on the velocity gradient near the wall, ($\tau_w = \mu(\frac{\partial u}{\partial y})$). Surprisingly the quality of the surface representation (case C in Section 4.3) were shown to be less important. The prism layer around the blades gave a $y^+ \approx 1$ but since the surface mesh had to be fine enough to represent the geometry even the models not including a prism layer had low y^+ values. The constant expansion of case C may for this particular case give a fine enough resolution in the near blade region but since this is dependent on the surface mesh it cannot be generally confirmed. Also notable is the relatively large amount of cells needed for the fan model. More than half of the total number of cells are used to represent the fan.

5.1 Recommendations

In order to secure a reliable method for flow rate prediction some further validation is recommended mainly for the fan model. A suggestion is to isolate the fan and try to reproduce fan performance data from the supplier or from internal testing. This would give a clearer view of the characteristics of the fan for varying loads and flow rates and would exclude the uncertainties connected with leakage of the complete test set up.

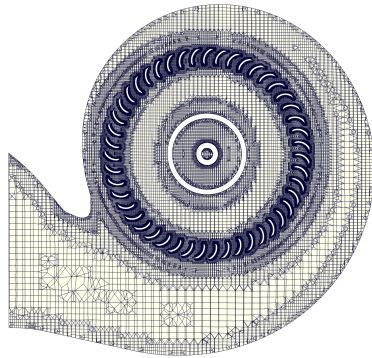
It is not possible to exclude that some of the instability encountered when simulating lower rotational speeds are a consequence of poor mesh quality. Therefore, a continued mesh dependency analysis should preferably be performed to exclude this possibility. Such analysis would probably make it possible to reduce the number of cells and speed up the convergence rate. As a suggestion a different mesh application could be used for better control of the near wall mesh.

References

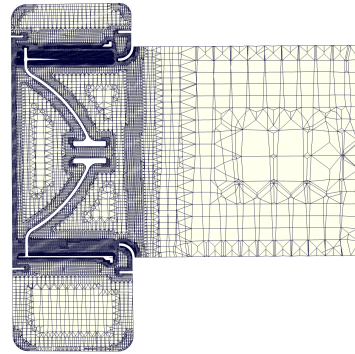
- [1] ANSYS *FLUENT Theory Guide*. Version 12.0. ANSYS, Inc, 2009.
- [2] ANSYS *FLUENT User's Guide*. Version 12.0. ANSYS, Inc, 2009.
- [3] I. Advanced Thermal Solutions. *Selecting a Fan for Your Thermal Management System*. 2011. URL: <http://qats.com/cms/2011/06/15/selecting-a-fan-for-your-thermal-management-system-part-2-of-2/>.
- [4] J. D. Anderson et al. *Computational Fluid Dynamics: An Introduction*. Ed. by J. F. Wendt. Springer-Verlag Berlin Heidelberg, 1996.
- [5] M. Bel-Hassan, A. Sardar, and R. Ghias. *CFD Simulations of an Automotive HVAC Blower: Operating under Stable and Unstable Flow Conditions*. Apr. 2008. DOI: 10.4271/2008-01-0735. URL: <http://dx.doi.org/10.4271/2008-01-0735>.
- [6] L. Davidson. *Fluid mechanics, turbulent flow and turbulence modeling*. 2013. URL: http://www.tfd.chalmers.se/~lada/postscript_files/solids-and-fluids_turbulent_flow_turbulence-modelling.pdf (visited on 05/22/2013).
- [7] L. Davidson. *Tensors*. 2011. URL: http://www.tfd.chalmers.se/~lada/turbulent_flow/postscript_files/chapter_tensorer.pdf (visited on 05/22/2013).
- [8] J. B. Evans. *Fan Selection and Sizing to Reduce Inefficiency and Low Frequency Noise Generation*. 2003. URL: <http://www.jeacoustics.com/library/pdf/72-Evans.pdf>.
- [9] P. Gullberg and R. Sengupta. *Axial Fan Performance Predictions in CFD, Comparison of MRF and Sliding Mesh with Experiments*. Apr. 2011. DOI: 10.4271/2011-01-0652. URL: <http://dx.doi.org/10.4271/2011-01-0652>.
- [10] E.-Y. Kwon et al. *Some Aerodynamic Aspects of Centrifugal Fan Characteristics of an Automotive HVAC Blower*. Mar. 2001. DOI: 10.4271/2001-01-0291. URL: <http://dx.doi.org/10.4271/2001-01-0291>.
- [11] A. K. M and K. Kanniah. *Flow and Pressure Drop Characteristics for Various Non-Circular Curved Ducts Used in Automobile HVAC System with Different Bend Angles*. Apr. 2013. DOI: 10.4271/2013-01-1645. URL: <http://dx.doi.org/10.4271/2013-01-1645>.
- [12] C. Online. *Introduction to turbulence*. 2012. URL: <http://www.cfd-online.com/Wiki/Turbulence> (visited on 05/22/2013).
- [13] A. Patidar, S. Natarajan, and M. Pande. *CFD Analysis and Validation of an Automotive HVAC System*. Apr. 2009.
- [14] T. M. Sales. *Air Flow Sensors*. URL: <http://www.autoshop101.com/forms/h34.pdf>.
- [15] S. J. S. University. *Fan Performance and Selection*. URL: <http://www.engr.sjsu.edu/ndejong/Fan%20Performance%20and%20Selection.pdf>.
- [16] H. K. Versteeg and W. Malalasekera. *An Introduction to Computational Fluid Dynamics: The Finite Volume Method*. First. Pearson Education Limited, 2007.
- [17] F. M. White. *Fluid Mechanics*. Sixth. McGraw-Hill, 2009.

Appendix A - Mesh Density

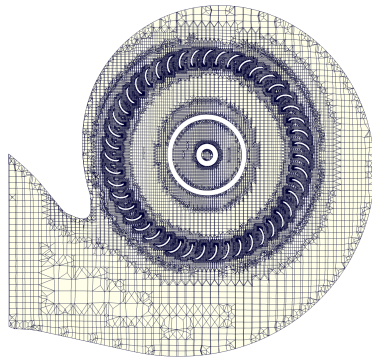
Figure 1 shows cross sections of the volume mesh of the fan for each of the different meshes. Figure 2 shows how the octree mesh propagates through the domain and how it refines towards the fan blades.



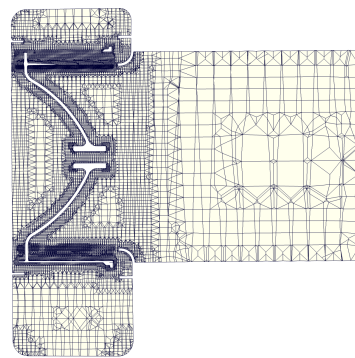
(a) *A mesh rad 1*



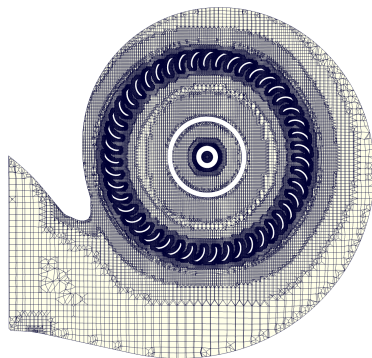
(b) *A mesh axial*



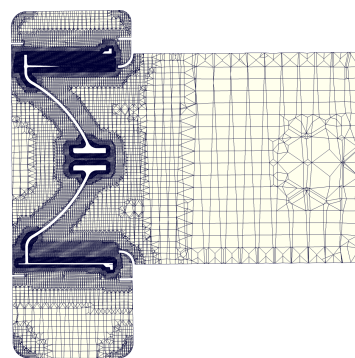
(c) *B mesh rad 1*



(d) *B mesh axial*

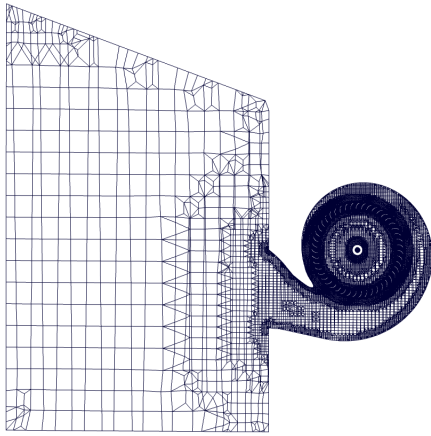


(e) *C mesh rad 1*

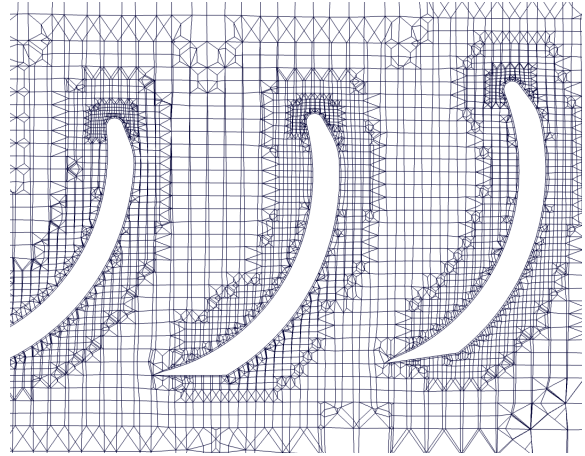


(f) *C mesh axial*

Figure 1: *Meshes for case A, B and C respectively*



(a) *Mesh propagation throughout the domain*



(b) *Mesh refining towards the blades*

Figure 2: *Mesh in domain and refinements towards blades*

Appendix B - Measurement

Figure 3 shows the data from the measurements. The lower part of the figure displays the flow through each individual nozzle and the upper one shows the total flow through the first row and the total leakage to the second row. Each step represents a increase in fan velocity (expressed in rpm). The airflow is shown on the y-label and is expressed in kg per hour. The x-label shows the time in seconds.

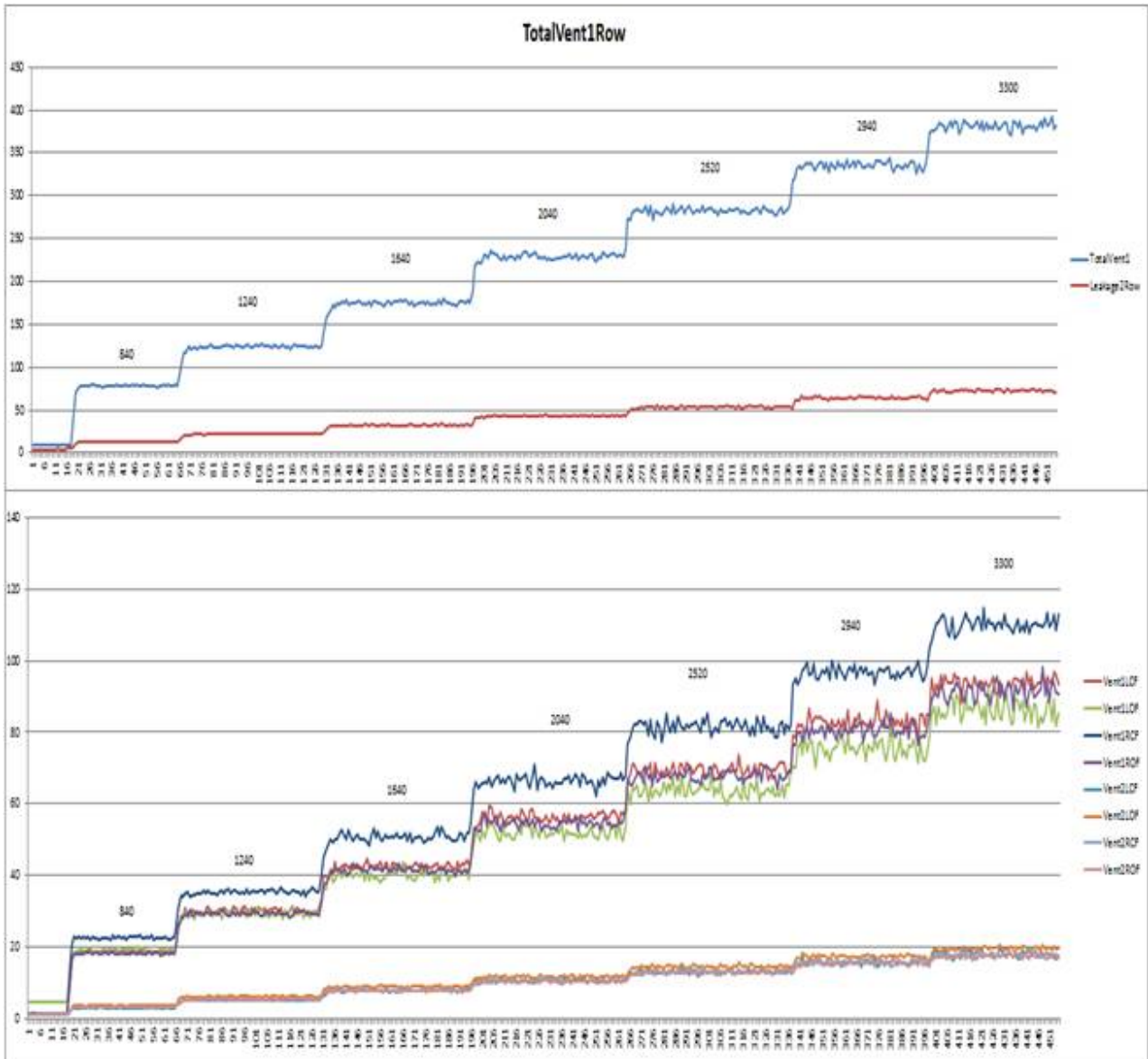


Figure 3: Collected data from measurements